Embedment Mechanism and Formulation of Major Types of Traditional Wooden Joints in Japan

H. Tanahashi & Y. Suzuki
Ritsumeikan University, Japan

SUMMARY:
There are many traditional wooden buildings, such as temples, shrines and town houses in Japan. Their structural systems are much different from modern structures. The major seismic resisting elements of the traditional wooden buildings are restoring forces of column rocking, rotational resistances of column-tie beam joints and shear resistances of mud/wood walls. Among them, the column-tie beam joints show the most ductile restoring force characteristics due to embedment and friction. We have already established Elasto-plastic Pasternak Model in order to formulate the restoring force characteristics of joints. However, there are many types of column-tie beam joints which may differ in mechanisms. Thus, we suggest the basic concept "Diagonal Effect" in order to analyze many types of traditional wooden joints effectively, and classify them into some major types and analyze their mechanisms. Moreover, we confirm the formulation with some experiments.

Keywords: Traditional wooden joint, restoring force characteristics, Pasternak Model, Diagonal Effect

1. INTRODUCTION

There are many traditional wooden buildings, such as temples, shrines and town houses in Japan. Some of them are registered as World Heritage. As a sample, Grand Gate of Itsukushima Shrine is shown in Fig. 1.1. Such wooden buildings should be prevented from probable damages caused by great earthquakes in the near future. In these decades, the seismic evaluation method of traditional wooden buildings has been researched actively by many institutions and researchers, and useful findings have been obtained. However, it has not been established so far because their structural systems, which have been succeeded and developed for a long time by carpenters, are much different from modern structures. Also, their seismic resistances are supposed to be insufficient in many cases. Therefore, it is urgently required to establish the evaluation method and seismic reinforcements by revealing such systems based on modern structural mechanics.

Figure 1.1. How to analyze this joint?

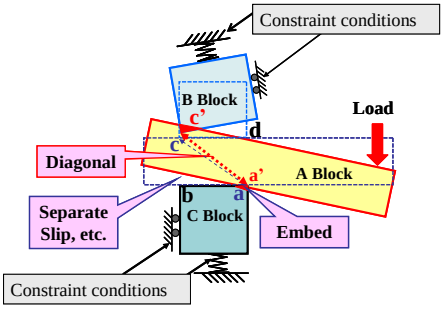

Figure 1.2. Concept of "Diagonal Effect"

The major seismic resisting elements of traditional wooden buildings are restoring forces of column rocking, rotational resistances of column-tie beam joints and shear resistances of mud/wood walls.

Among them, in general, the column-tie beam joints show the most ductile restoring force characteristics due to embedment and friction inside the joints, although their rotational stiffness is rather small.
Therefore, we made clear the yielding/hardening mechanism of embedment of wood perpendicular to the grain and applied **P**asternak **M**odel (abbreviated to PM) to the elasto-plastic embedment behaviour of traditional wooden joints and developed **E**lasto-plastic **P**asternak **M**odel (abbreviated to EPM) for the restoring force characteristics of joints. Moreover, we verified the formulation with some experiments of basic types of joints [Tanahashi et al., 2010, 2011a, b].
However, there are many types of column-tie beam joints which may differ in mechanisms and deformability. Some of them are complicate in details and their systems are very difficult to understand. Thus, we suggest the basic concept "Diagonal Effect" of Fig. 1.2. in order to analyze many types of traditional wooden joints effectively, and classify them into some major types and analyze their mechanisms from a viewpoint of stiffness, strength and deformability. Moreover, we confirm the formulation with some experiments [Tanahashi et al., 2012].

2. DIAGONAL EFFECT AND MAJOR TYPES OF JOINTS

We introduce the basic concept "Diagonal Effect" as shown in Fig. 1.2. In general, traditional wooden joints are composed of some cubic wooden blocks A, B, C etc. interlocked each other in three dimensions. If an external load is applied to the joint, each block contacts, embeds, slips and separates, depending on the constraint conditions and material characteristics of blocks. Now, we aim at the movement of the polygon **abcd** and the diagonal from **ac** to **a'c'** shown in red dotted arrow. This red dotted arrow represents the major movement and the key point of the behaviour of this joint.
The constraint conditions are the same as boundary conditions in mechanical analyses, however, there are very few fixed, pin or roller supports in these cases. In many cases, joints are composed of free cubic bodies, and boundary conditions are continuously distributing supports or contacts with nonlinearity. Moreover, in general, the wooden blocks are anisotropic continua and nonlinear materials with large variations. Therefore, the mechanical solution of the joints is complicate and very difficult to solve in general.
Of course, finite element method (FEM) or distinct element method (DEM) may solve such mechanical problems, however, only numerical solutions are obtained, and closed-form explicit solutions cannot be obtained in general. In order to formulate the restoring force characteristics of joints, approximate mechanical models which can give closed-form solutions are required.
Based on above discussions, we reconsider the mechanism of joints from primitive types to developed ones, and we have suggested the basic concept on the mechanisms of joints focusing on "Diagonal Effect" in order to approach the solution [Tanahashi et al., 2012]. This keyword helps us to understand the mechanisms of traditional wooden joints.
As a result, we summarized that the most basic mechanisms of traditional wooden joints are three types as; *Nuki* type, *Yatoi* type and strut type. If we analyze these three types, we can easily access the more complex types of joints which are combined with basic types. Thus, we introduce the three types of joints briefly and establish the formulation of the restoring force characteristics of the *Nuki* and *Yatoi* type and confirm it with *Yatoi* type experiments.

2.1. *Nuki* type

The *Nuki* is a kind of tie beam, which means "penetrating beam" in Japanese. This type is rather simple and it consists of a column with mortise and a *Nuki* penetrating through the mortise, and the wedges are used usually in order to tighten the joint as shown in the *Nuki* specimen in Fig. 2.1.
The mechanism is shown in Fig. 2.2. If a moment is applied to the joint, the column inclines and embedment takes place at the *Nuki* surface because the Young's modulus of column parallel to the grain is several ten times larger than that of the *Nuki* perpendicular to the grain. The red triangles show embedded sections. Additionally the embedment takes place at the outside of the column edge because of wood as a continuum, and the reaction $\boldsymbol{R}_1$ becomes large due to the outside reaction. This increasing effect can be formulated by PM [Tanahashi et al., 2011a]. Frictional reaction is omitted here for

simplicity. The large deformability of the *Nuki* type has been confirmed as seen in Fig. 2.1.

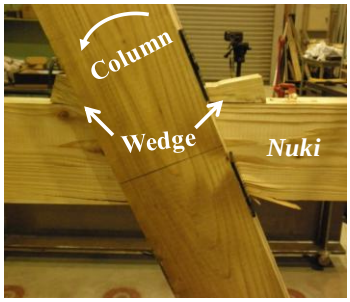

Figure 2.1. Large deformation of *Nuki* specimen

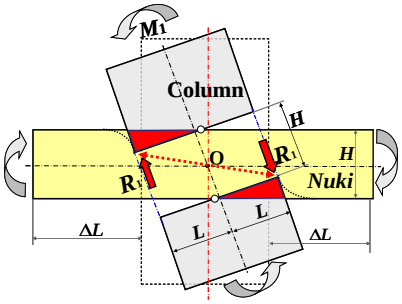

Figure 2.2. Mechanism of *Nuki* type

2.2. *Yatoi* type

The *Yatoi* type consists of the column sandwiched with separated and constrained beams as shown in Fig. 2.3. In many cases, the separated beams are combined by the *Yatoi* which means an "employed tenon" made of another wood piece, i.e., a spline tenon. The *Yatoi* is also connected with beams through the groove by "*Shachi-sen",* a kind of shear connector or cotter. The mechanism is shown in Fig. 2.4.

If a moment is applied to the joint, the column also inclines and embedment takes place at the column surface mainly due to the tensile force of the *Yatoi* connecting both beams with the *Shachi-sen* or cotter. However, the embedment depends on the embedment stiffness of column surface and the tensile stiffness of the *Yatoi* including the *Shachi-sen* or cotter. In general, the embedment triangle is rather small, thus the reaction $\boldsymbol{R}_2$ becomes smaller than $\boldsymbol{R}_1$ of the *Nuki* type comparatively.

The *Yatoi* height is half of the beam and thin in general, thus, it can penetrate easily across the lower *Yatoi* without too large mortise of columns. Comparing to the *Nuki*, the details are fit for a large column with tie beams crossing in two ways. Also, beams can be prepared for each column spacing and built up easily.

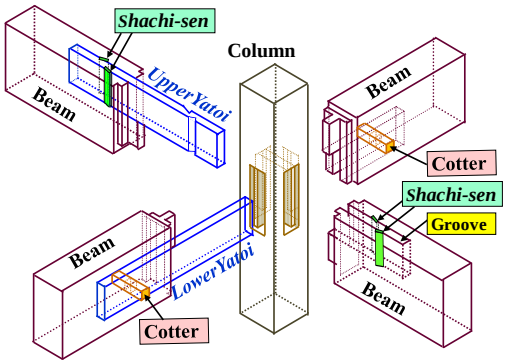

Figure 2.3. Details of *Yatoi* type

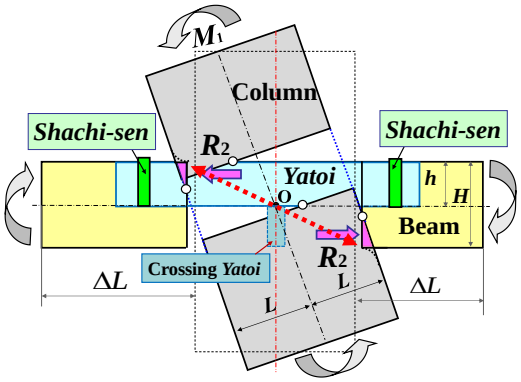

Figure 2.4. Mechanism of *Yatoi* type

However, this mechanism is not perfectly analyzed yet so far because of complicate details as shown in Fig. 2.3. Therefore, we show the general mechanism, then, propose our simulation for this type of mechanism in the following chapter.

2.3. Strut type

The strut type of joints is shown in Fig. 2.5. This type is found in a strut or a short column supporting the beam even if there are no shear connectors. It rotated on the base or the beam, embedding into the beams under the constraints of the structure in Fig. 2.6., which are some results of shaking table tests or static loading tests of traditional wooden buildings. Although the same mechanism is found in

beams between columns, it has been mostly overlooked, however, it should be considered in some cases. In the case of the *Shachi-sen*, we can interpret that the inclined small block of the *Shachi-sen* rotates and embeds into the groove wall shown later in Fig. 4.6. Thus, the strut type will be applied to the failure mechanism of the *Shachi-sen.*

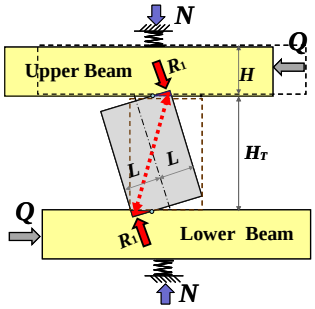

Figure 2.5. Mechanism of strut type

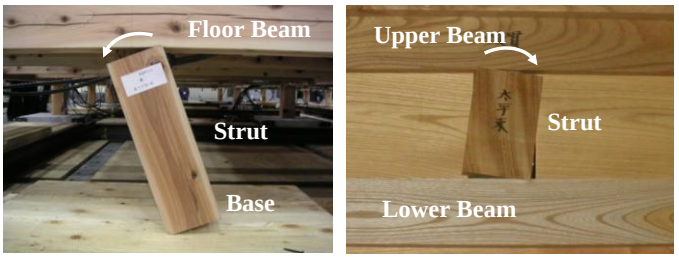

Figure 2.6. Deformation of strut on the base or the beam

3. GENERAL MECHANISM AND FORMULATION OF WOODEN JOINT

3.1. Elasto-plastic Pasternak Model formulation

Now, we introduce the general mechanism including *Nuki* and *Yatoi* types in Fig. 3.1. The difference is only the constraint conditions of upper and lower blocks if the column and beams are exchanged. The tensile stiffness *k*c is almost infinite for the *Nuki*, and it is finite for the *Yatoi*. As the column rotates around **O**, two blocks separate as δ_H assuming the line AB and A'B' to be parallel, then, the embedment takes place in red triangles. Therefore, the formulation is established in the same manner as shown in Eqns. 3.1-3.12, referring to Fig. 3.2. The embedment surface is expressed by *W*, that is, Abc in Eqn. 3.1. Ab is a straight line and bc is an exponential curve based on the PM formulation. The reaction of this embedment area is $\boldsymbol{R_1}$, and the moment $\boldsymbol{M_R}$ is given by the integral of moment of the red hatched zone around **O** in Eqn. 3.5.
Frictional reaction $\boldsymbol{F_1}$ occurs at the contact surface between the tenon and mortise. It works along the line AB and A'B' and is evaluated as Coulomb friction. This moment $\boldsymbol{M_F}$ is expressed in Eqn. 3.6. It is noted the horizontal reaction $\boldsymbol{R_H}$ also works at the point B due to the increased contact length *dL*. This component is very important for large deformability of joint, however, it is difficult to estimate this reaction quantitatively. Thus, it is evaluated experimentally so far.

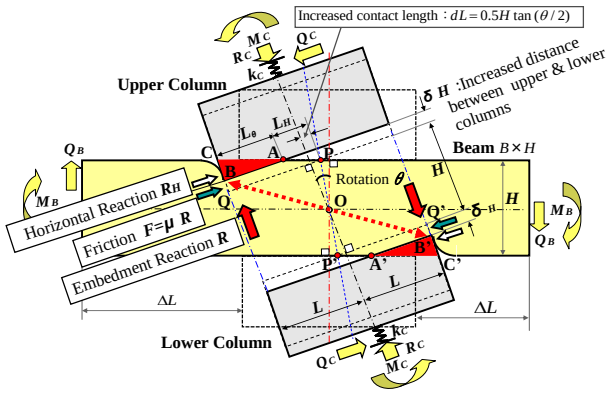

Figure 3.1. Mechanism of *Nuki* and *Yatoi* type

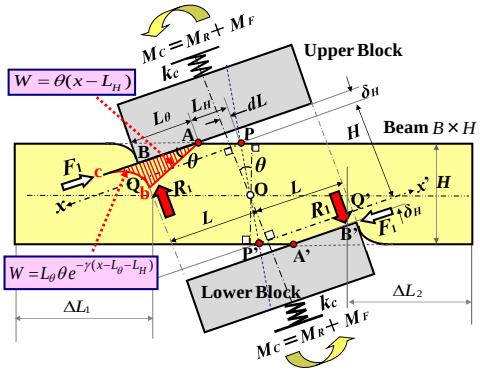

Figure 3.2. Mechanical model for formulation

In both elastic and plastic states, we can simulate the moment ***M***-elasto-plastic rotation angle $\boldsymbol{\theta_p}$ relation in Eqns. 3.13-3.20. This formulation is extended to rotational embedment from partial compression [Tanahashi et al., 2011a].

Embedded displacement W by EPM due to rotation angle θ for the *Nuki* and *Yatoi* type:

$$\boldsymbol{W} = \begin{cases} \theta(x - L_H) & : L_H \le x \le L_\theta + L_H, \\ L_\theta \theta e^{-\gamma(x - L_\theta - L_H)} & : x \ge L_\theta + L_H, \end{cases} \quad (3.1)$$

where, $L_\theta = L + dL - L_H$: contact length at rotation angle θ, (3.2)

$2\delta_H$: Increased distance between upper and lower columns,

$\rho = (L - L_\theta)/L_\theta, \quad L_H = \delta_H / \tan\theta, \quad dL = 0.5H \tan(\theta/2),$ (3.3)

B : Breadth of *Nuki* / Beam, H : Height of *Nuki* / Beam,

$2L$: Depth of column, ΔL : End distance,

E : Compressive Young's modulus of *Nuki* / Beam perpendicular to the grain,

γH : Non-dimendional characterisitc value of PM,

μ : Coefficient of friction,

$k = E/H$: Compressive stiffness of *Nuki* / Beam.

Normal reaction $\boldsymbol{R_1}$ due to rotational embedment:

$$\boldsymbol{R_1} = \int_{L_H}^{\infty} kWBdx = \frac{EBL_\theta^{\,2}}{2H}\left(1 + \frac{2(1 - e^{-\gamma\Delta L})}{\gamma L_\theta}\right)\theta = \frac{EBL_\theta^{\,2}}{2H}\zeta_N\theta = K_{N0}\zeta_N\theta. \quad (3.4)$$

Moment $\boldsymbol{M_R}$ due to rotational embedment:

$$\begin{aligned} \boldsymbol{M_R} &= 2\int_{L_H}^{\infty} kWBxdx = \frac{2EBL_\theta^{\,3}}{3H}\left\{1 + 1.5\rho + \frac{3}{\gamma L_\theta}\left[\left(1 + \rho + \frac{1}{\gamma L_\theta}\right)\left(1 - e^{-\gamma\Delta L}\right) - \frac{\Delta L}{L_\theta}e^{-\gamma\Delta L}\right]\right\}\theta \\ &= \frac{2EBL_\theta^{\,3}}{3H}\zeta_R\theta = K_{R0}\zeta_R\theta. \end{aligned} \quad (3.5)$$

Moment $\boldsymbol{M_F}$ due to friction of rotational embedment:

$$\boldsymbol{M_F} = \mu R_1(H + 2\delta_H) = \mu\frac{EBL_\theta^{\,2}}{2H}(H + 2\delta_H)\zeta_F\theta = \mu K_{F0}\zeta_F\left(1 + \frac{2\delta_H}{H}\right)\theta, \quad (3.6)$$

$K_{N0} = \dfrac{EBL_\theta^{\,2}}{2H}$: Basic stiffness in compression, (3.7)

$\zeta_N = 1 + \dfrac{2(1 - e^{-\gamma\Delta L})}{\gamma L_\theta}$: Stiffness increasing factor in compression, (3.8)

$K_{R0} = \dfrac{2EBL_\theta^{\,3}}{3H}$: Basic stiffness in rotation, (3.9)

$\zeta_R = 1 + 1.5\rho + \dfrac{3}{\gamma L_\theta}\left[\left(1 + \rho + \dfrac{1}{\gamma L_\theta}\right)\left(1 - e^{-\gamma\Delta L}\right) - \dfrac{\Delta L}{L_\theta}e^{-\gamma\Delta L}\right]$: Stiffness increasing factor in rotation, (3.10)

$K_{F0} = \dfrac{EBL_\theta^{\,2}}{2}$: Basic stiffness in rotational friction, (3.11)

$\zeta_F = 1 + \dfrac{2(1 - e^{-\gamma\Delta L})}{\gamma L_\theta}$: Stiffness increasing factor in rotational friction. (3.12)

Elasto-plastic rotation $\boldsymbol{\theta_p}$ due to $\boldsymbol{M_R}$, $\boldsymbol{M_F}$:

$$\boldsymbol{\theta_P} = \frac{\boldsymbol{M_R} + \boldsymbol{M_F}}{K_{R0}\zeta_R(\theta) + \mu K_{F0}\zeta_F(\theta)}, \tag{3.13}$$

$$\left.\begin{aligned} \zeta_R(\theta) &= \frac{\zeta_R}{1+mh_y} \quad : \text{Stiffness function of rotation,} \\ \zeta_F(\theta) &= \frac{\zeta_F}{1+mh_y} \quad : \text{Stiffness function of friction,} \end{aligned}\right\} \tag{3.14}$$

$$m = C(1-\frac{\theta_y}{\theta\eta}) = C(1-\frac{1}{\kappa}) \ : \text{Equivalent multiplying factor,} \tag{3.15}$$

C : Plastic strain multiplier,

$$h_y = \frac{1}{\eta}\ln(\frac{\theta\eta}{\theta_y}) = \frac{1}{\eta}\ln\kappa : \text{Yielding depth ratio } (0 \le h_y \le 1), \tag{3.16}$$

$$\text{where, } \kappa = \frac{\theta\eta}{\theta_y} = \frac{\varepsilon\eta}{{}_F\varepsilon_y} : \text{Yielding ratio,} \tag{3.17}$$

$$\eta : \text{Parameter of strain profile,} \tag{3.18}$$

$$W\phi' = \varepsilon\eta e^{-\eta\frac{z}{H}} = \varepsilon\phi_S \quad : \text{Strain profile,} \tag{3.19}$$

$$\phi_S = \eta e^{-\eta\frac{z}{H}} : \text{Shape function of strain profile.} \tag{3.20}$$

As for the strut type, it is possible to formulate similarly, however, we will treat it elsewhere because of some different situations.

3.2. Some additional problems for *Yatoi* type joints

We have already verified our formulation by joint tests in the case of *Nuki* [Tanahashi et al., 2011b, 2012], however, there are some problems in the case of *Yatoi*. One is the evaluation of the tensile stiffness $k_c (= k_y \text{ for } Yatoi)$ including the *Shachi-sen* or cotter. In the *Yatoi* joint, the contact length L_θ is obtained by the solution of Eqn. 3.22 based on the load balance and the assumption of k_y, δ_H and $\gamma L_\theta \cong \text{constant}$ as follows.

$$R_1 = k_y\delta_H, \quad \delta_H = (L + dL - L_\theta)\tan\theta \cong (L + dL - L_\theta)\theta, \tag{3.21}$$

$$\frac{EBL_\theta{}^2}{2H}(1 + \frac{2}{\gamma L_\theta})\theta = k_y(L + dL - L_\theta)\theta, \tag{3.22}$$

Thus, $$L_\theta = -(l + \frac{1}{\gamma}) + \sqrt{(l + \frac{1}{\gamma})^2 + 2l(L + dL)}, \quad \text{where, } l = \frac{k_y H}{EB}. \tag{3.23}$$

The other is that the *Yatoi* itself has some stiffness and resistance as a kind of *Nuki*. Of course, it depends on the tightness and constraint conditions.
In *Yatoi* details, "*Mechigai*" is another important component of joints. *Mechigai* means a shallow tenon with 15mm depth usually protruding into the column in Fig. 4.2. This detail works as a kind of *Nuki* and a shear connector in the horizontal direction for preventing the *Shachi-sen* from failure shown later.

4. EXPERIMENTAL RESULTS AND SIMULATION OF *YATOI* JOINT

4.1. Summary of cross type loading tests of *Yatoi* joints

Horizontal loading tests of the cross type *Yatoi* joint were carried out by the Committee of the Structural Design Code and its Verification Experiment on Japanese Traditional Wooden Structures.
The test setup is drawn in Fig. 4.1. Used materials are; columns and beams: Japanese cedar (*E*=6GPa:Young's modulus parallel to the grain), *Yatoi*: Japanese cypress (*E*=9GPa) and *Shachi-sen*: Oak (*E*=16GPa). *Shachi-sen* is slightly tapered and the joint becomes tighten like a wedge by driving it down. The dimensional parameters of three different size specimens are shown in Table 4.1., referring to Fig. 4.2. Cyclic loadings for positive and negative directions were controlled three times at the same deformation angle of 1/480, 1/240, 1/120, 1/90, 1/60, 1/45, 1/20, 1/15 rad. Displacements and rotations of the joint, *Yatoi*, and *Shachi-sen* were measured by displacement transducers.

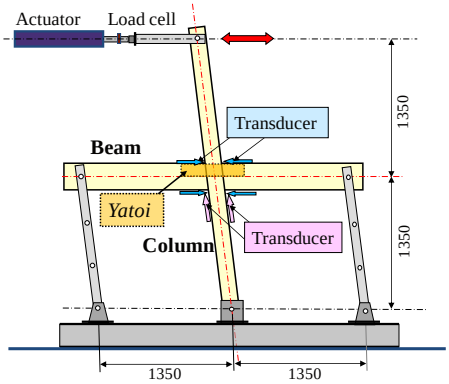

Figure 4.1. Test setup of *Yatoi* joint

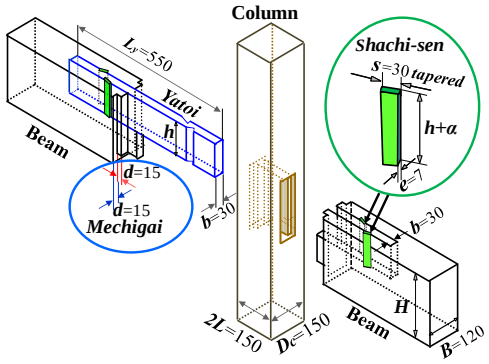

Figure 4.2. Dimensions of test specimens

Table 4.1. List of test specimens

Specimen	Column	Beam		*Yatoi*			*Shachi-sen*			*Mechigai*	Number
	Depth	Breadth	Height	Breadth	Height	Length	Height	Depth	Breadth	Depth	of specimen
	$2L\,(=D_c)$	*B*	*H*	*b*	*h*	L_y	*h*	*e*	*s*	*d*	*n*
A-1	150	120	300	30	150	550	150+α	7	30	15	3
A-2	150	120	240	30	120	550	120+α	7	30	15	3
A-3	150	120	150	30	75	550	75+α	7	30	15	3

4.2. Test results and analysis of mechanism

Three different sizes of joint behaved almost similarly and three specimens of the same sizes had small variations. Therefore, a typical ultimate deformation of Specimen A-2-2 at the rotation angle θ =0.1rad is shown for analysis in Fig. 4.3.
We assumed mechanisms from the embedded deformation in Fig. 4.4 and drawn three kinds of embedment triangles and reactions in red, blue and purple triangles. Three mechanisms are simplified and illustrated separately in Fig. 4.5. The deformed details and failure state are drawn in Fig. 4.6.
1) M1 is column embedment mechanism; Reaction is $\boldsymbol{R}_1$ at the red triangles which are assumed point-symmetric. In this simulation, the dimensional parameters must be used according to Fig. 4.2. As the beam height for simulation is 150mm of the column depth in all specimens, the effective embedment breadth of the beam is *B-b*=90mm, and the effective column depth for simulation is 300mm for A-1, 240mm for A-2 and 150mm for A-3, which correspond to the beam height.
2) M2 is *Mechigai* embedment mechanism; Reaction is $\boldsymbol{R}_2$ at the blue triangles where the narrow surfaces of *Mechigai* of beam ends embed together with outside surface of the column edge. The effective embedment breadth of beam is *B-b-2d* =60mm and the depth is *H* of Table 4.1. The embedment stiffness is supposed to be small due to complex body of the *Yatoi* and the beam.
3) M3 is *Yatoi* embedment mechanism; Reaction is $\boldsymbol{R}_3$ at the purple triangles where the *Yatoi* embeds at the upper left surface and the lower right surface of the *Yatoi*. However, the latter is around middle of the column, whose embedment stiffness is rather small due to complex body of the *Yatoi*, beam and column without wedges, and is difficult to evaluate.
Yatoi itself plays the definitely important role in M1and M2 as a tensile member and in M3 as an embedment member.

Figure 4.3. Deformed Specimen A-2-2(0.1rad)

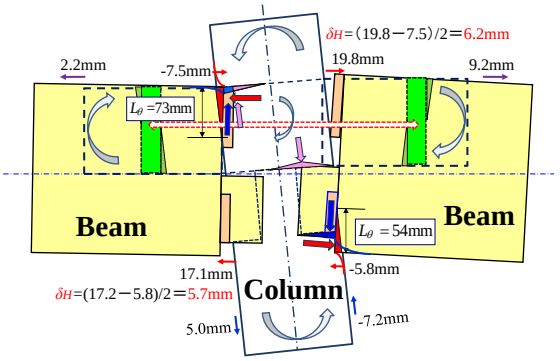

Figure 4.4. Supposed reactions inside the joint

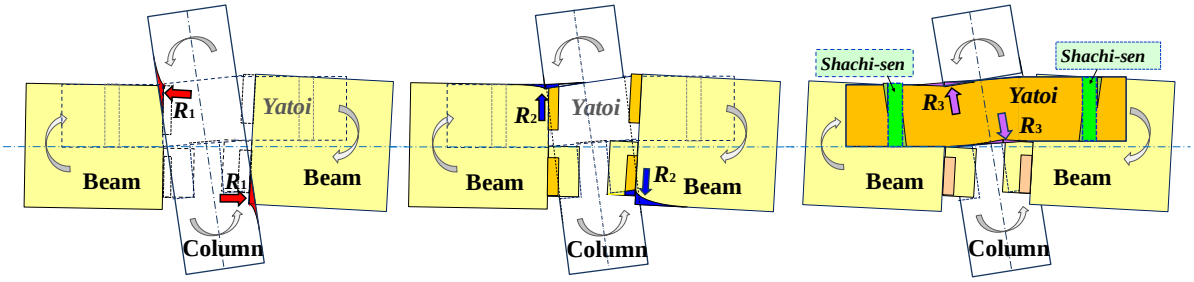

M1: Column embedment M2: *Mechigai* embedment M3: *Yatoi* embedment

Figure 4.5. Three mechanisms of *Yatoi* joint

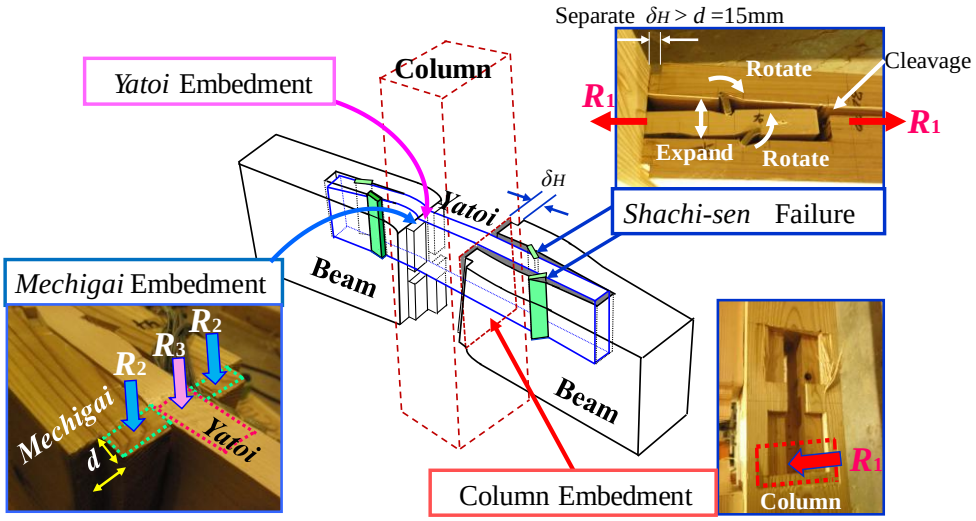

Figure 4.6. Deformation and failure mechanism of *Yatoi* joint A-2-2

4.3. EPM simulation

Based on the above analysis, we simulated the restoring force characteristics of each mechanism and summed them up and show the results of Specimen A-2-2, A-1-1 and A-3-1 in Figs. 4.7-4.9. The red star means the ultimate state, which are not simulated so far. The probable parameters for EPM simulations were assumed according to the previous embedment test results and some case studies on Specimen A-2-2 in order to fit the deformations. The same parameters were applied to the other sizes and simulated results of L_θ, δ_H, $M_{\theta u}$ (moment at ultimate rotation angle θ_u) and $M_{all}=M_1+M_2+M_3$ are shown in Table 4.2. The formulation can simulate them fairly well in both elastic and plastic states,

though Specimen A-1-1 is underestimated a little. However, the ratios of the restoring forces of three mechanisms depend on the Young's moduli perpendicular to the grain, the tightness of contact interfaces of joints and so forth. Therefore, these simulations are results from probable case studies and the parameters for EPM simulations may be refined based on further researches.

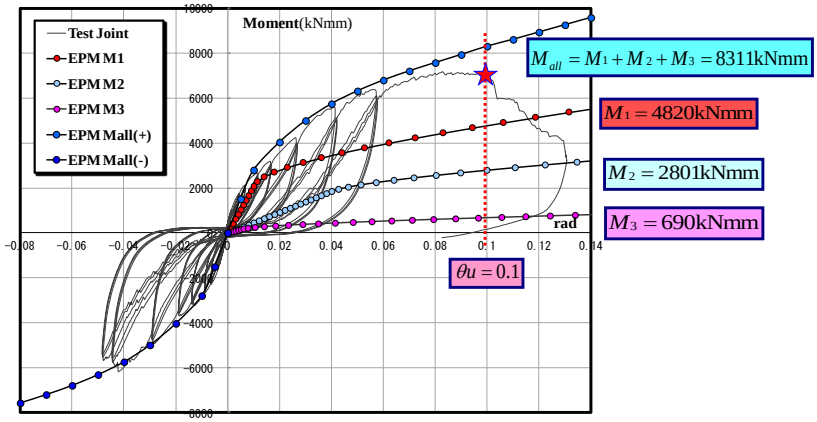

Figure 4.7. EPM simulation of Specimen A-2-2

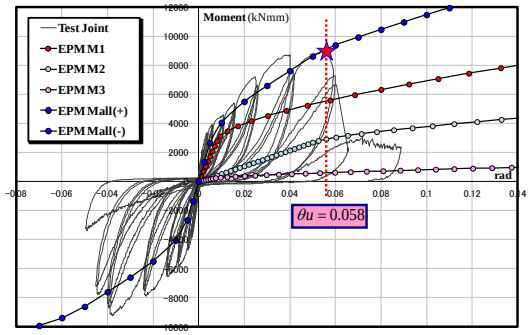

Figure 4.8. EPM simulation of A-1-1

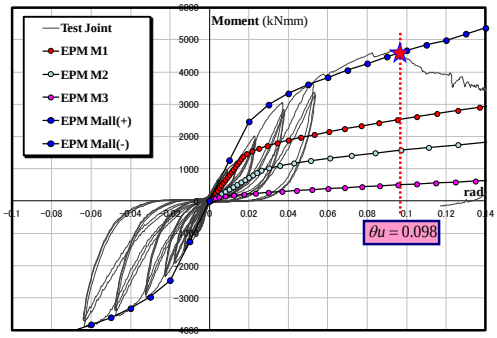

Figure 4.9. EPM simulation of A-3-1

Table 4.2. Parameters for EPM simulation

Specimen	Mechanism	E(MPa)	ε_y	σ_y(MPa)	γH	η	C	μ	k_y(kN/mm)	L_θ(mm)	δ_H	$M_{\theta u}$(kNmm)	M_{all}(kNmm)
	M1	200	0.015	3.0	2.8	1.8	15	0.5	9.0	58.2	6.7	M_1=4820	
A-2-2	M2	50	0.03	1.5	2.5	2.4	15	0.5	—	—	—	M_2=2801	8311
	M3	200	0.005	1.0	3.0	2.4	8	0.5	—	—	—	M_3= 690	
	M1	200	0.015	3.0	2.8	1.8	15	0.5	11.25	76.3	4.8	M_1=5708	
A-1-1	M2	50	0.03	1.5	2.5	2.4	15	0.5	—	—	—	M_2=3050	9415
	M3	200	0.005	1.0	3.0	2.4	8	0.5	—	—	—	M_3= 657	
	M1	200	0.015	3.0	2.8	1.8	15	0.5	5.65	33.1	4.5	M_1=2561	
A-3-1	M2	50	0.03	1.5	2.5	2.4	15	0.5	—	—	—	M_2=1605	4666
	M3	200	0.005	1.0	3.0	2.4	8	0.5	—	—	—	M_3= 500	

4.4. Failure mechanism and deformability

The maximum restoring forces of the *Yatoi* joint were observed at the time when the *Shachi-sen* rotated and expanded the groove of the beam horizontally, and the interlocked *Mechigai* with the column was released as shown Fig. 4.6. As a result, the *Yatoi* failed when the *Mechigai* came out more than 15mm from the column surface. At the groove end, a cleavage failure occurred and also, the *Shachi-sen* failed in compression, shearing or buckling. In some cases, the side wall of the groove split

due to Diagonal Effect of the *Shachi-sen*. Therefore, many failure modes took place. However, maximum moments took place almost at the rotation angle θ_u=0.06～0.1rad for A-2, $\theta_u \cong$0.06rad for A-1 and $\theta_u \cong$0.1 for A-3. In general, this deformability was less than cross type *Nuki* which can deform more than 0.2rad as shown in Fig. 2.1.
Since the separation of *Mechigai d*=15mm from column surface worked as a trigger of failure, it is possible to increase the deformability if the *Mechigai* depth *d* is designed more than 15mm which has been decided by carpenters conventionally. Of course, we should consider the failure of column and beams in addition to the failure of joints for the whole structure.
As for the mechanism of the *Shachi-sen* failure, it is similar to the Diagonal Effect of the strut, thus it is possible to simulate the *Shachi-sen* by EPM simulation.

5. CONCLUSIONS

The main conclusions of this research are summarized as follows.

1) There are many types of traditional wooden joints in Japan and some of their mechanisms are not well understood so far because of complexity in details. In order to understand complicate types of joints, we suggested basic concept "Diagonal Effect" and classified them into three basic types of joints and analyzed them. We conclude that the basic concept "Diagonal Effect" is effective to understand the complex mechanisms of traditional wooden joints.
2) We analyzed the test results of the *Yatoi* type and shown three components of embedment mechanisms as M1, M2 and M3. Then, we applied EPM formulation for the three mechanisms and simulated them in order to verify the formulation and discussed. As a result, the proposed mechanisms and formulation can simulate the restoring force characteristics of *Yatoi* type joints fairly well in both elastic and plastic states. However, the assumed parameters may be refined based on further investigations.
3) The failure mechanism of the *Yatoi* joint is mainly due to the rotational failure of the *Shachi-sen* which depends on the *Mechigai* depth, shearing, buckling of the *Yatoi* itself, cleavage of groove and so on.
4) We are going to continue further experiments and simulations for other types of joints including the struts, some small blocks of the *Shachi-sen*, shear connectors, wedges and so forth.

ACKNOWLEDGEMENTS

Experimental results were obtained by the Committee of the Structural Design Code and its Verification Experiment on Japanese Traditional Wooden Structures (Chairman: Yoshiyuki Suzuki, Professor of Ritsumeikan University). We would like to thank the committee members for their cooperation.
This research was also supported in part by Ritsumeikan University Global COE Program for Education, Research and Development of Strategy on Disaster Mitigation of Cultural Heritage and Historic Cities, MEXT, Japan and by the Grant-in-Aid for Scientific Research (S) from Japan Society for the Promotion of Science [No.19106010].

REFERENCES

Tanahashi, H. and Suzuki, Y.(2010). Elasto-plastic Pasternak Model simulation of static and dynamic loading tests of traditional wooden frames. *World Conference on Timber Engineering 2010.* **Paper ID 508**.

Tanahashi, H., Ooka, Y., Izuno, K. and Suzuki, Y.(2011a). Yielding mechanism of embedment of wood and formulation of elasto-plastic embedded displacements. *Journal of Structural and Construction Engineering.* **76:662**,811-819, (in Japanese).

Tanahashi, H. and Suzuki, Y.(2011b). Characteristics of elasto-plastic rotational embedment of traditional wooden joints and formulation of crosspiece joints. *Journal of Structural and Construction Engineering.* **76:667**, 1675-1684, (in Japanese).

Tanahashi, H. and Suzuki, Y.(2012). Basic concept and general formulation of restoring force characteristics of traditional wooden joints. *World Conference on Timber Engineering 2012*. (submitted).